Detection of primary angle closure suspect with different mechanisms of angle closure using multivariate prediction models

Ye Zhang,[1,†] Zhe Dong,[1,†] Qing Zhang,[2] Lei Li,[1] Ravi Thomas,[3,4] Si Zhen Li,[5] Ming Guang He[6,7,8] and Ning Li Wang[1,2] iD

[1]Beijing Tongren Eye Center, Beijing Key Laboratory of Ophthalmology and Visual Science, Beijing Tongren Hospital, Capital Medical University, Beijing, China
[2]Beijing Institute of Ophthalmology, Beijing, China
[3]Queensland Eye Institute, Brisbane, Australia
[4]University of Queensland, Brisbane, Australia
[5]Nanjing Tongren Hospital, Nanjing, China
[6]State Key Laboratory of Ophthalmology, Zhongshan Ophthalmic Center, Sun Yat-sen University, Guangzhou, China
[7]Department of Surgery, University of Melbourne, Melbourne, Australia
[8]Ophthalmology, Centre for Eye Research Australia, Melbourne, Australia

ABSTRACT.

Purpose: We had found that a multivariate prediction model used for the detection of primary angle-closure suspects (PACS) by combining multiple static and dynamic anterior segment optical coherence tomography (ASOCT) parameters had an area under the receiver operating characteristic curve (AUC) of 0.844. We undertook this study to evaluate this method in screening of PACS with different dominant mechanisms of angle closure (AC).

Methods: The right eyes of subjects aged ≥40 years who participated in the 5-year follow-up of the Handan Eye Study and had undergone gonioscopy and ASOCT examinations under light and dark conditions were included. All ASOCT images were analysed by the Zhongshan Angle Assessment Program. The dominant AC mechanism in each eye was determined to be pupillary block (PB), plateau iris configuration (PIC) or thick peripheral iris roll (TPIR). Backward logistic regression (LR) was used for inclusion of variables in the prediction models. LR, Naïve Bayes' classification (NBC) and neural network (NN) were evaluated and compared using the AUC.

Results: Data from 796 subjects (413 PACS and 383 normal eyes) were analysed. The AUCs of LR, NBC and NN in the PB group were 0.920, 0.918 and 0.917. The AUCs of LR, NBC and NN in the PIC group were 0.715, 0.708 and 0.707. The AUCs of LR, NBC and NN in TPIR group were 0.867, 0.833 and 0.886.

Conclusions: Prediction models showed the best performance for detection of PACS with PB mechanism for AC and have potential for screening of PACS.

Key words: primary angle-closure suspect – screening – angle-closure mechanisms – static and dynamic ASOCT parameters – prediction models

Introduction

Glaucoma is a leading cause of irreversible blindness worldwide, and primary angle-closure glaucoma (PACG) is a major cause of visual impairment in Asia, especially in China (Quigley et al. 2006; Tham et al. 2014). With 10 million people estimated to be affected with PACG in China by 2020 (about 48% of the total worldwide), the disease will be a serious challenge for healthcare systems in our country (Quigley et al. 2006).

The definition of primary angle-closure disease (PACD) and the diagnosis of primary angle-closure suspect (PACS), primary angle closure (PAC) and primary angle-closure glaucoma (PACG) were based on the criteria established by the International Society of Geographic and Epidemiologic Ophthalmology (ISGEO) (Foster et al. 2002).

Vision loss resulting from PACG cannot be reversed; it is therefore essential to detect the early asymptomatic stage of the disease (PACS) and perform prophylactic laser iridotomy to prevent damage to the optic nerve and irreversible visual impairment (Weinreb et al. 2006; Tham et al. 2014).

Gonioscopy is the gold standard examination for opportunistic case

detection in clinics (Fu et al. 2019). For the evaluation of anterior chamber angle, gonioscopy permits direct visualization of angle structures (Qiao et al. 2019). However, gonioscopy is a relatively subjective technique with substantial intra- and inter-observer variability, requires considerable expertise and involves topical anaesthesia as well as contact with the cornea (Friedman et al. 2008; Lavanya et al. 2008). All these limit the use of gonioscopy in population-based screening (Lavanya et al. 2008).

Several non-contact imaging devices of the anterior chamber angle (ACA) are available, but none were considered an ideal screening test for PACS (Zhang et al. 2014).

Anterior segment optical coherence tomography (ASOCT) uses an infrared light with a wavelength of 1310 nm and provides non-contact in vivo crosssectional imaging of the anterior segment of the eye in the absence of visible light spectrum influence on angle configuration and pupil size, either qualitatively or through various quantitative parameters. It has high axial resolution and short acquisition time (Radhakrishnan et al. 2001; Friedman et al. 2008). This technique assesses the ACA, iris, and lens parameters objectively and is capable of recording transient and dynamic changes of the pupil at low levels of illumination (Radhakrishnan et al. 2001; Moghimi et al. 2013).

As ASOCT can visualize the entire anterior chamber, all the essential parameters for detection of angle closure (AC)/narrow angle can be examined in a single scan, which makes the ASOCT a potential tool to screen for PACS without relying on a specialist performing gonioscopy (Dorairaj et al. 2012).

We recently evaluated the diagnostic ability of three prediction models based on static and dynamic ASOCT parameters to detect PACS as an early screening tool (unpublished data). A neural network (NN) model with a variable set consisting of 4 ASOCT-derived parameters – angle recess area at 750 μm (ARA750) in light, lens vault (LV) in light, anterior chamber volume (ACV) in light and iris cross-sectional area (IA) change/ pupil diameter (PD) change – had the largest area under the receiver operating characteristic curve (AUC) of 0.844 in

identifying eyes with gonioscopic PACS. While this is a good AUC, it is still not ideal for population-based screening. A possible reason for this was considered to be different angle-closure mechanisms of PACS eyes enrolled in that study.

The aim of this investigation was to evaluate three prediction models to detect PACS with different dominant AC mechanisms including pupillary block (PB), plateau iris configuration (PIC) and thick peripheral iris roll (TPIR), based on static and dynamic ASOCT parameters.

Methods

This was a cross-sectional observational study conducted with the approval of the Ethics committee of the Beijing Tongren Hospital. We adhered to the tenets of Declaration of Helsinki, and informed consent was obtained from all participants.

Subjects aged ≥40 years who participated in the five-year follow-up examination of the Handan Eye Study (HES) between June 2012 and May 2013, with limbal anterior chamber depth ≤40%, and had undergone gonioscopic examination and ASOCT imaging under light and dark conditions were eligible for inclusion.

Patients were excluded if they had a history of use of eyedrops that could influence the anterior chamber angle, intraocular surgery, laser treatment, eye trauma and ocular surface disorders, such as corneal opacity, pterygium or other abnormalities that precluded ASOCT imaging. Eyes with peripheral anterior synechiae (PAS), raised intraocular pressure (IOP), cup–disc ratio ≥0.6 or presence of typical glaucomatous optic neuropathy (GON), secondary AC, and past history of acute angle-closure (AAC) attack were also excluded. Other exclusion criteria were inability to fixate on the target, or general physical or mental impairment that precluded participation in the testing.

All participants underwent a comprehensive ophthalmic examination including presenting visual acuity (PVA) and best-corrected visual acuity (BCVA) measurement using a logarithm of minimum-angle-of-resolution chart (LogMAR E chart), auto-refraction (Topcon KR-8800, Topcon Corporation, Tokyo, Japan), slit-lamp

examination, IOP using Kowa applanation tonometry, A-scan ultrasound biometry using an OcuScan RxP (Alcon, Inc., Fort Worth, TX, USA) and stereoscopic optic-disc examination with a 90-dioptre lens (Volk Optical Inc., Mentor, OH, USA).

Gonioscopy

Gonioscopy was performed in the dark in all enrolled subjects by one of two glaucoma specialists (ZP and YSH) who were masked to imaging findings. Static gonioscopy was performed using a Goldmann one-mirror lens at a magnification of ×16 with the eye in the primary position of gaze. Care was taken to avoid light falling on the pupil and to avoid inadvertent indentation during examination. Dynamic examination (manipulation) then was performed using the same lens. Primary angle-closure suspects (PACS) was diagnosed if ≥180° of the posterior trabecular meshwork was not visible on static gonioscopy.

ASOCT imaging and measurement

The Visante ASOCT (Carl Zeiss Meditec Inc., Dublin, CA, USA) obtains scans at a rate of 2000 A-scans per second, with an axial and transverse resolution of 18 and 60 μm, respectively (Quek et al. 2011).

Subjects underwent ASOCT imaging first under dark conditions (~3 lux, to induce physiologic mydriasis) after allowing dark adaptation for at least 3 min prior to examination without the use of any mydriatics followed by imaging under light conditions (~200 lux). The scans were performed by a single trained examiner who was masked to the gonioscopy results. During ASOCT scanning, an internal fixation target was used with the subjects' refractive correction in place to perform the measurements in an unaccommodated state.

All images were obtained in the 'anterior segment quadrant' mode at 0°–180°, 45°–225°, 90°–270°, and 135°–315° meridians. Due to interference from the eyelids with image acquisition of the ACA at 6 and 12 o'clock, the lower lid was gently retracted by the operator to image the inferior angle and the upper lid was elevated gently to image the superior angle; care was taken to avoid pressure on the globe.

Imaging was repeated if the scleral spur visibility was poor.

A customized software, the Zhong-shan Angle Assessment Program (ZAAP, Guangzhou, China), was used to process the ASOCT images (Console et al. 2008). For each image, one ophthalmologist (ZY) determined the location of the 2 scleral spurs, described as the inward protrusion of the sclera with a change in curvature of its inner surface (Sakata et al. 2008). The algorithm then automatically calculated parameters, including angle opening distance at 500 μm (AOD500), trabecular-iris space area at 500 μm (TISA500), angle recess area at 750 μm (ARA750), anterior chamber depth (ACD), anterior chamber area (ACA), anterior chamber volume (ACV), anterior chamber width (ACW), iris thickness at 750 μm (IT750), iris curvature (IC) and iris cross-sectional area (IA), lens vault (LV), and pupil diameter (PD) (Console et al. 2008).

The AOD500 was measured as the perpendicular distance between anterior iris surface and a point at trabecular meshwork at 500 μm anterior to the scleral spur (Salim 2012). The TISA500 was measured as an area bounded anteriorly by the AOD500, posteriorly by a line drawn from the scleral spur perpendicular to the plane of the inner scleral wall to the opposing iris, superiorly by the inner corneoscleral wall and inferiorly by the iris surface (Salim 2012). The ARA750 is the area of the angle recess bounded anteriorly by the anterior iris surface, corneal endothelium and a line perpendicular to the corneal endothelium drawn to the iris surface from a point at 750 μm anterior to the scleral spur (Salim 2012).

The ACD was measured as the perpendicular distance from the corneal endothelium at the corneal apex to the anterior lens surface (Salim 2012). The ACA was defined as the cross-sectional area of anterior segment bounded by the corneal endothelium, the anterior surface of the iris and the anterior surface of the lens (within the pupil) (Wang et al. 2012). The algorithm plots a vertical axis through the midpoint (centre) of the anterior chamber area, and by rotating the anterior chamber area 360 degrees around this vertical axis, calculates the ACV (Wang et al. 2012). The ACW was

defined as the horizontal scleral spur-to-spur distance (Nongpiur et al. 2010).

The IT750 was the iris thickness measured at 750 μm from the scleral spur, and the IC was determined by measuring the maximum distance between the posterior iris surface and a line from the iris root to the first point of contact between the iris and lens (Wang et al. 2013). The LV was the perpendicular distance between the anterior pole of the crystalline lens and the horizontal line joining the 2 scleral spurs (Nongpiur et al., 2011a).

The IA was calculated as the cross-sectional area of the full length (from spur to pupil) of the iris (Sun et al. 2012). Iris cross-sectional area (IA) change was calculated as IA in light minus IA in dark, and PD change was calculated as PD in dark minus PD in light. Iris cross-sectional area (IA) change/PD change was calculated as IA change divided by PD change.

Categories of angle-closure mechanisms

Four ASOCT images from each PACS eye obtained in the dark with clearly discernible scleral spurs were analysed qualitatively and categorized into one of three AC mechanisms: PB, PIC and TPIR (Figs 1, 2 and 3). Where the image suggested more than one

mechanism for AC, a forced choice was made to select the dominant mechanism without the benefit of other information. The AC mechanism that was identified in at least two ASOCT images of each PACS eye was determined to be predominant AC mechanism of that eye. The detailed guidelines of the three AC mechanism categorizations based on ASOCT images and the reproducibility of AC mechanism categories based on ASOCT and ultrasound bio-microscopy (UBM) images are described elsewhere (Zhang et al. 2015; Zhang et al. 2016).

Statistical analysis

Data from right eyes of all the enrolled subjects were analysed using the Statistical Analysis System (SAS) version 9.4 (SAS Institute, Cary, NC, USA). For continuous variables, data were first examined by Kolmogorov–Smirnov test for the normality of distribution. Variables demonstrating a normal distribution were presented as mean (standard deviation, SD), while variables failing to achieve a normal distribution were presented as median (percentiles). For those variables with a normal distribution, analysis of variance (ANOVA) was used to compare the
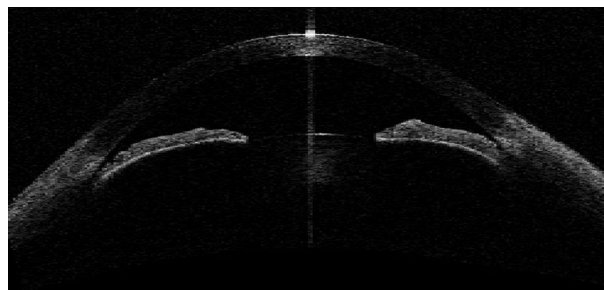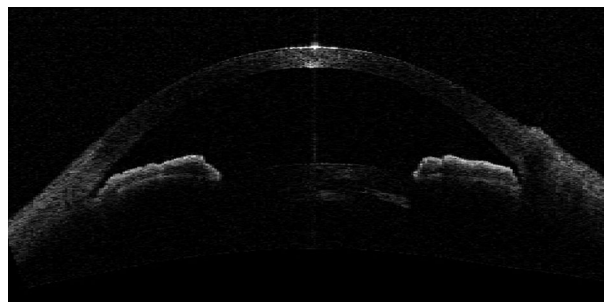

Fig. 1. Angle-closure mechanism – pupillary block.

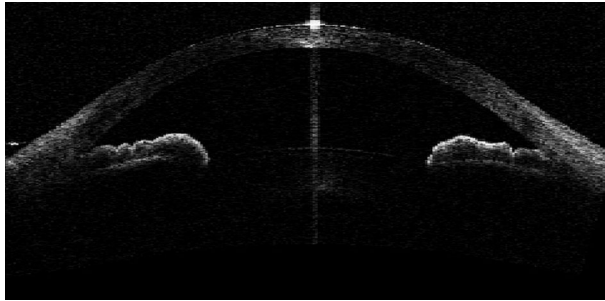**Fig. 2.** Angle-closure mechanism – plateau iris configuration.

Fig. 3. Angle-closure mechanism – thick peripheral iris roll.

Fig. 4. Angle-closure mechanism – exaggerated lens vault.

difference between four groups: normal subjects and PACS patients with the three different AC mechanisms. Bonferroni correction was used to adjust p-values for multiple pair-wise comparisons of normally distributed variables. The Kruskal–Wallis test for unpaired data was used to compare variables which were not normally distributed and to determine differences between the four groups. The Mann–Whitney U-test was used to compare the normal group and PACS groups with PB, PIC or TPIR, respectively. A p value < 0.05 was considered statistically significant.

Variable selection

Normal subjects were classified as negative outcomes. For each PACS group with PB, PIC or TPIR, logistic regression (LR) analysis (Backward) was used for inclusion of variables in the prediction models from the following 12 parameters under dark and light conditions: AOD500, TISA500, ARA750, IT750, IC, LV, ACD, ACW, ACA, ACV, IA and PD. And plus two calculated parameters of changes in dark and light conditions including IA change and IA change/ PD change, there were a total of 26 candidate parameters for inclusion of variables in the prediction models. First of all, we used the univariate LR analysis (Backward) on the 26 ASOCT parameters and excluded the variables with a p value more than 0.1.

Then, in order to avoid the obvious correlations between the independent variables, we designed four combinations of variables for multivariate LR analysis (Backward) to build the models for each PACS group with different

Table 1. Demographic and ocular bircometric data of PACS subjects with different angle-closure mechanisms and normal subjects.

Parameter	1 = PB (n = 141)	2 = PIC (n = 147)	3 = TPIR (n = 125)	0 = Normal Subjects (n = 383)	p value	p value (0 & 1)	p value (0 & 2)	p value (0 & 3)
Age, median (IR), years	64.0 (59.0, 70.0)	60.0 (55.0, 64.0)	62.0 (57.0, 66.5)	61.0 (56.0, 66.0)	<0.001[†]	<0.001[§]	0.079[§]	0.190[§]
Male (%)	36 (25.5)	48 (32.7)	43 (34.4)	145 (37.9)	0.067[‡]			
Female (%)	105 (74.5)	99 (67.3)	82 (65.6)	238 (62.1)				
PVA, median (IR)	0.34 (0.20, 0.50)	0.20 (0.08, 0.40)	0.30 (0.14, 0.44)	0.20 (0.10, 0.32)	<0.001[†]	<0.001[§]	0.898[§]	0.001[§]
BCVA, median (IR)	0.10 (0.00, 0.21)	0.00 (0.00, 0.15)	0.10 (0.00, 0.17)	0.00 (0.00, 0.16)	<0.001[†]	<0.001[§]	0.699[§]	0.058[§]
SE, median (IR), dioptre	1.00 (0.13, 1.75)	0.75 (0.00, 1.50)	0.63 (0.00, 1.50)	0.50 (−0.13, 1.13)	<0.001[†]	<0.001[§]	0.018[§]	0.027[§]
IOP, median (IR), mmHg	11.3 (10.0, 13.0)	12.0 (10.0, 13.5)	12.0 (10.0, 13.0)	12.0 (10.0, 13.5)	0.148[†]			
CCT, median (IR), μm	527 (512, 544)	528 (514, 552)	530 (514, 548)	528 (513, 546)	0.568[†]			
Central ACD, median (IR), mm	2.44 (2.30, 2.68)	2.58 (2.43, 2.84)	2.47 (2.31, 2.71)	2.71 (2.49, 2.92)	<0.001[†]	<0.001[§]	0.002[§]	<0.001[§]
LT, median (IR), mm	4.97 (4.69, 5.16)	4.73 (4.39, 4.94)	4.90 (4.48, 5.15)	4.78 (4.48, 5.07)	<0.001[†]	<0.001[§]	0.092[§]	0.093[§]
AL, median (IR), mm	22.19 (21.81, 22.75)	22.29 (21.89, 23.15)	22.23 (21.61, 22.80)	22.73 (22.22, 23.25)	<0.001[†]	<0.001[§]	<0.001[§]	<0.001[§]

ACD = anterior chamber depth, AL = axial length, BCVA = best-corrected visual acuity, CCT = central corneal thickness, IOP = intraocular pressure, IR = interquartile range, LT = lens thickness, PB = pupillary block, PIC = plateau iris configuration, PVA = presenting visual acuity, SE = spherical equivalent, TPIR = thick peripheral iris roll.
[†] Kruskal–Wallis test.
[‡] χ^2 test.
[§] Mann–Whitney test (<0.05/4 = 0.0125 = significant different).

AC mechanisms: 1. 12 parameters under light conditions plus IA change; 2. 12 parameters under light conditions plus IA change/PD change; 3. 12 parameters under dark conditions plus IA change; and 4. 12 parameters under dark conditions plus IA change/ PD change. The variance inflation factors (VIFs) and clinical significance of included factors were calculated and considered to determine the included variables in multivariate logistic regression analysis. Significant variables with a p value less than 0.1 in the multivariate analysis were finally selected. The Nagelkerke R squares were calculated to evaluate and to select the best one that fitted the data from the four combinations of each PACS group with different AC mechanisms.

Prediction model development

We randomly split the dataset into two samples: 70% for the training (or derivation) set and 30% for the testing (or validation) set. We used the training subsets to develop and evaluate the three prediction models for the detection of gonioscopic PACS with three different AC mechanisms: logistic regression (LR), Naïve Bayes' classification (NBC), and neural network (NN) (Hastie et al. 2009). All the significant variables selected through univariate and multivariate LR analysis were used to build the three prediction models.

Logistic regression is a probabilistic model that uses the relationship between dependent and independent variables as a concrete function for prediction models (Cox 1958). We first ran the LR models by SAS 9.4 using the significant variables selected for detection of PACS with different AC mechanisms. This was our baseline statistical model, as logistic regression is the usual and standard method for binary classification in epidemiological research and clinical applications (Ford et al. 2019).

The Naïve Bayes model, which is a probabilistic model that predicts output, calculates the probability that a given instance belongs to a certain class by using the Bayesian theorem (McCallum et al. 1998). Naïve Bayes' classification (NBC) is fast and easy to build, and useful for the classification of large datasets (Jamal et al. 2020). In our study, Naïve Bayes models for

Table 2. ASOCT data of PACS subjects with different angle-closure mechanisms and normal subjects.

Conditions	Parameter	1 = PB (n = 141)	2 = PIC (n = 147)	3 = TPIR (n = 125)	0 = Normal Subjects (n = 383)	p value	p value (0 & 1)	p value (0 & 2)	p value (0 & 3)
Light	AOD500, median (IR), mm	0.210 (0.158, 0.281)	0.285 (0.232, 0.363)	0.217 (0.156, 0.292)	0.339 (0.276, 0.434)	<0.001†	<0.001§	<0.001§	<0.001§
	TISA500, median (IR), mm²	0.095 (0.074, 0.118)	0.118 (0.099, 0.145)	0.090 (0.065, 0.122)	0.142 (0.116, 0.177)	<0.001†	<0.001§	<0.001§	<0.001§
	ARA750, median (IR), mm²	0.262 (0.189, 0.344)	0.309 (0.250, 0.378)	0.227 (0.164, 0.310)	0.390 (0.311, 0.475)	<0.001†	<0.001§	<0.001§	<0.001§
	ACD, median (IR), mm	2.113 (1.964, 2.249)	2.378 (2.243, 2.545)	2.264 (2.104, 2.393)	2.488 (2.325, 2.642)	<0.001†	<0.001§	<0.001§	<0.001§
	ACW, median (IR), mm	10.79 (10.47, 11.06)	11.02 (10.79, 11.28)	10.85 (10.60, 11.10)	11.12 (10.82, 11.43)	<0.001†	<0.001§	0.021§	<0.001§
	ACA, median (IR), mm²	14.72 (13.19, 15.92)	17.13 (15.97, 18.74)	15.84 (14.16, 17.08)	18.27 (16.60, 19.82)	<0.001†	<0.001§	<0.001§	<0.001§
	ACV, median (IR), mm³	56.25 (48.64, 63.11)	67.83 (61.96, 75.40)	59.49 (52.44, 66.87)	73.89 (65.25, 82.40)	<0.001†	<0.001§	<0.001§	<0.001§
	IT750, median (IR), mm	0.44 (0.39, 0.47)	0.45 (0.42, 0.48)	0.50 (0.47, 0.55)	0.44 (0.39, 0.48)	<0.001†	0.616§	0.324§	<0.001§
	IC, mean (SD), mm	0.30 (0.06)	0.24 (0.07)	0.25 (0.06)	0.24 (0.07)	<0.001*	<0.001‡	1.000‡	1.000‡
	LV, median (IR), mm	499.8 (413.8, 587.7)	326.9 (220.2, 449.5)	398.4 (292.8, 509.7)	269.1 (119.0, 409.5)	<0.001†	<0.001§	<0.001§	<0.001§
Dark	AOD500, median (IR), mm	0.176 (0.124, 0.233)	0.258 (0.204, 0.328)	0.178 (0.110, 0.260)	0.307 (0.242, 0.383)	<0.001†	<0.001§	<0.001§	<0.001§
	TISA500, median (IR), mm²	0.075 (0.055, 0.099)	0.103 (0.076, 0.128)	0.068 (0.045, 0.101)	0.127 (0.100, 0.156)	<0.001†	<0.001§	<0.001§	<0.001§
	ARA750, median (IR), mm²	0.191 (0.140, 0.256)	0.257 (0.181, 0.327)	0.168 (0.109, 0.256)	0.322 (0.253, 0.405)	<0.001†	<0.001§	<0.001§	<0.001§
	ACD, median (IR), mm	2.123 (1.967, 2.246)	2.385 (2.255, 2.547)	2.258 (2.080, 2.399)	2.483 (2.329, 2.636)	<0.001†	<0.001§	<0.001§	<0.001§
	ACW, median (IR), mm	10.93 (10.65, 11.19)	11.03 (10.79, 11.30)	10.91 (10.59, 11.14)	11.11 (10.84, 11.39)	<0.001†	<0.001§	0.066§	<0.001§
	ACA, median (IR), mm²	15.16 (13.58, 16.43)	17.54 (16.52, 19.19)	15.97 (14.46, 17.45)	18.61 (16.89, 20.27)	<0.001†	<0.001§	<0.001§	<0.001§
	ACV, median (IR), mm³	58.01 (49.91, 64.93)	69.70 (63.62, 77.25)	60.14 (52.42, 69.20)	74.57 (66.57, 83.86)	<0.001†	<0.001§	<0.001§	<0.001§
	IT750, median (IR), mm	0.47 (0.41, 0.50)	0.48 (0.45, 0.51)	0.53 (0.50, 0.57)	0.47 (0.42, 0.51)	<0.001†	0.431§	0.076§	<0.001§
	IC, median (IR), mm	0.29 (0.25, 0.32)	0.23 (0.19, 0.28)	0.24 (0.21, 0.28)	0.24 (0.20, 0.28)	<0.001†	<0.001§	0.291§	0.311§
	LV, median (IR), mm	552.7 (422.0, 684.6)	341.7 (204.6, 446.0)	412.4 (276.2, 530.8)	285.9 (138.5, 401.6)	<0.001†	<0.001§	0.003§	<0.001§

ACA = anterior chamber area, ACD = anterior chamber depth, ACV = anterior chamber volume, ACW = anterior chamber width, AOD500 = angle opening distance at 500 µm, ARA750 = angle recess area at 750 µm, IC = iris curvature, IR = interquartile range, IT750 = iris thickness at 750 µm, LV = lens vault, PB = pupillary block, PIC = plateau iris configuration, SD = standard deviation, TISA500 = trabecular-iris space at 500 µm, TPIR = thick peripheral iris roll.
* One-way analysis of variance.
† Kruskal–Wallis test.
‡ Bonferroni.
§ Mann–Whitney test (<0.05/4 = 0.0125 = significant different).

detection of PACS with different AC mechanisms were developed by SAS 9.4 using the significant variables.

Neural network mimics the brain's information processing system, which involves complex neuron connections and complex computations (Hassoun 1995). Neural network (NN) consists of multiple linear regression models are advantageous when there is a large number of variables with complex relations among them (Dreiseitl et al. 2002). For each PACS group, significant variables selected were used as inputs and 1 binary variable (PACS or normal) was used as output. Our NN models, which were built by the Statistical Package for Social Sciences (SPSS) version 25.0 (SPSS, Chicago, IL, USA), consisted of one input layer, a hidden layer and an output layer.

The ROC curve was used as a metric to measure prediction model performance. Each model was assessed for its ability to classify PACS cases versus controls using the AUCs. The optimal operating point was determined at the point at which the Youden index was maximized and was used as the diagnostic threshold to calculate sensitivity and specificity (Fluss et al. 2005). The estimates of AUC (95% confidence interval [CI]), sensitivity and specificity were obtained using the SPSS 25.0. Comparisons of AUCs of the three different models for each PACS group with PB, PIC or TPIR were performed using ANOVA.

The testing dataset was used to validate models' ability to discriminate between PACS patients versus normal subjects. Overall model accuracy which is the correct classification ratio for each model was the key indicator of model validation in our study.

Results

Subjects characteristics

A total of 989 subjects age ≥40 years who attended the 5-year HES follow-up and completed ocular examinations as well as gonioscopy and ASOCT measurements under light and dark conditions were eligible for inclusion. A total of 132 eyes (13.3%) were excluded due to poor quality ASOCT images or inability to accurately identify the scleral spur.

We excluded 5 PACS eyes considered to have an exaggerated lens vault

Table 3. Changes in IA, IV and PD from light to dark conditions in PACS subjects with different angle-closure mechanisms.

Parameter	1 = PB (n = 141)	2 = PIC (n = 147)	3 = TPIR (n = 125)	0 = Normal Subjects (n = 383)	p value	p value (0 & 1)	p value (0 & 2)	p value (0 & 3)	p value (1 & 2)	p value (1 & 3)	p value (2 & 3)
IA; L, mean (SD), mm^2	2.76 (0.38)	2.89 (0.40)	3.05 (0.39)	2.94 (0.37)	<0.001*	<0.001‡	0.658‡	0.078‡	0.031‡	<0.001‡	0.004‡
PD; L, median (IR), mm	3.89 (3.39, 4.34)	3.90 (3.41, 4.33)	3.95 (3.55, 4.42)	3.89 (3.41, 4.34)	0.234*	0.109‡	1.000‡	0.004‡	1.000‡	<0.001‡	0.002‡
IA; D, mean (SD), mm^2	2.63 (0.37)	2.68 (0.40)	2.84 (0.35)	2.71 (0.36)	<0.001*						
PD; D, median (IR), mm	4.73 (4.25, 5.18)	4.81 (4.34, 5.24)	4.81 (4.38, 5.29)	4.83 (4.22, 5.26)	0.256*						
IA Change, median (IR), mm^2	0.13 (−0.02, 0.29)	0.22 (0.07, 0.37)	0.21 (0.03, 0.35)	0.24 (0.09, 0.37)	<0.001†	<0.001§	0.532§	0.237§	0.001§	0.005§	0.608§
PD Change, median (IR), mm	0.64 (0.51, 0.96)	0.81 (0.58, 1.16)	0.70 (0.53, 1.03)	0.79 (0.55, 1.15)	0.012†	0.004§	0.561§	0.309§	0.003§	0.004§	0.159§
IA Change/PD Change, median (IR), mm	0.15 (−0.03, 0.33)	0.25 (0.10, 0.39)	0.24 (0.05, 0.39)	0.26 (0.15, 0.38)	<0.001†	<0.001§	0.299§	0.345§	0.007§	0.009§	0.945§

IA Change = IA in light − IA in dark; PD Change = PD in dark − PD in light.
D = dark, IA = iris cross-sectional area, IR = interquartile range, L = light, PB = pupillary block, PD = pupil diameter, PIC = plateau iris configuration, SD = standard deviation, TPIR = thick peripheral iris roll.
* One-way analysis of variance.
† Kruskal–Wallis test.
‡ Bonferroni.
§ Mann–Whitney test (<0.05/4 = 0.0125 = significant different).

(Fig. 4) as the dominant AC mechanism and 13 PACS eyes in which the dominant AC mechanism could not be identified. Data from the right eye of 796 subjects including 413 PACS and 383 normal subjects were included in the final analysis. There were no statistically significant differences in demographic or ocular features between the included and excluded subjects. A total of 141 PACS eyes were determined to have PB (34.1%), 147 PACS eyes PIC (35.6%) and 125 PACS eyes TPIR (30.3%) as the dominant AC mechanism.

The demographic and ocular biometric data of subjects with each AC mechanism group and normal group are shown in Table 1. There was no significant difference in sex, IOP and CCT among the four groups. A significant difference existed in age (p < 0.001), PVA (p < 0.001), BCVA (p < 0.001), spherical equivalent (SE) (p < 0.001), central ACD (p < 0.001), lens thickness (LT) (p < 0.001) and axial length (AL) (p < 0.001) between the four groups.

Quantitative anterior chamber parameters measured using ASOCT in the four groups in light and dark conditions along with the differences between the groups are summarized in Table 2. Significant differences across all parameters were found between the four groups in both light and dark conditions (p < 0.001).

Iris cross-sectional area measurements

A summary of mean IAs, PDs, IA changes, PD changes and IA changes/PD changes in light and dark conditions in four groups is shown in Table 3. Significant differences in IA's in light and dark (p < 0.001), changes in IA's (p < 0.001), changes in PD's (p = 0.012) and IA changes/PD changes (p < 0.001) in dark and light conditions were observed between the four groups. The PB group was found to have the smallest IA changes (p < 0.001 between PB and normal groups, p = 0.001 between PB and PIC groups, p = 0.005 between PB and TPIR groups) and IA changes/PD changes (p < 0.001 between PB and normal groups, p = 0.007 between PB and PIC groups, p = 0.009 between PB and TPIR groups).

Multivariate prediction models

For PACS group with PB, the Nagelkerke R^2 of the four combinations of variables selected through multivariate LR analysis are shown in Table 4, with the best one being 0.563. For PACS group with PIC, the parameter IA change was excluded through univariate LR analysis because of a P value of less than 0.1. Hence, there were only two combinations of variables, with the Nagelkerke R^2 being 0.178 and 0.157 (Table 4). Finally, for PACS group with TPIR, two parameters including IA change and IA change/PD change were both excluded through univariate LR analysis. There were also two combinations of variables left through multivariate LR analysis, with the Nagelkerke R^2 being 0.358 and 0.441 (Table 4).

Table 5 details the variables included as the best combinations using LR analysis. In the PB group, ACV in light (p < 0.001), LV in light (p < 0.001) and IA change/PD change (p < 0.001) were included. In the PIC group, significant variables were

Table 4. Nagelkerke R squares of different combinations of variables through backward logistic regression analysis

Angle-Closure Mechanisms	Logistic Models	Parameter	Nagerkerke R^2
Pupillary Block	1	ACV (L), LV (L), IA Change	0.553
	2	ACV (L), LV (L), IA Change/PD Change	0.563
	3	IC (D), ACV (D), LV (D), IA Change	0.554
	4	IC (D), ACV (D), LV (D), IA Change/PD Change	0.557
Plateau Iris Configuration	1	AOD500 (L), ARA750 (L), IA Change/PD Change	0.178
	2	ARA750 (D), ACD (D), LV (D), IA Change/PD Change	0.157
Thick Peripheral Iris Roll	1	ARA750 (L), IA (L), ACV (L)	0.358
	2	ARA750 (D), IT750 (D), ACV (D)	0.441

IA Change = IA in light – IA in dark; PD Change = PD in dark – PD in light.
ACD = anterior chamber depth, ACV = anterior chamber volume, AOD500 = angle opening distance at 500 μm, ARA750 = angle recess area at 750 μm, D = dark, IA = iris cross-sectional area, IC = iris curvature, IT750 = iris thickness at 750 μm, L = light, LV = lens vault, PD = pupil diameter.

Table 5. Variables included in the best combinations through backward logistic regression analysis

Angle-Closure Mechanisms	Parameter	Estimated regression coefficient	Standard error	χ^2	p value	OR (95% CI)
Pupillary Block	ACV; L, mm^3	−0.121	0.018	47.072	<0.001	0.886 (0.856, 0.917)
	LV; L, mm	0.005	0.001	24.450	<0.001	1.005 (1.003, 1.007)
	IA Change/PD Change, mm	−1.987	0.520	14.582	<0.001	0.137 (0.049, 0.380)
Plateau Iris Configuration	AOD500; L, mm	4.976	2.232	4.971	0.026	144.963 (1.825, 11512.382)
	ARA750; L, mm^2	−10.113	2.128	22.577	<0.001	<0.001 (<0.001, 0.003)
	IA Change/PD Change, mm	−0.803	0.368	4.770	0.029	0.448 (0.218, 0.921)
Thick Peripheral Iris Roll	ARA750; D, mm^2	−8.507	1.987	18.339	<0.001	<0.001 (<0.001, 0.010)
	IT750; D, mm	12.039	2.862	17.698	<0.001	169282.464 (620.373, 46192469.33)
	ACV; D, mm^3	−0.033	0.015	4.684	0.030	0.967 (0.939, 0.997)

IA Change = IA in light – IA in dark; PD Change = PD in dark – PD in light.
ACV = anterior chamber volume; AOD500 = angle opening distance at 500 μm; ARA750 = angle recess area at 750 μm; D = dark; IA = iris cross-sectional area; IT750 = iris thickness at 750 μm; L = light; LV = lens vault; PD = pupil diameter.
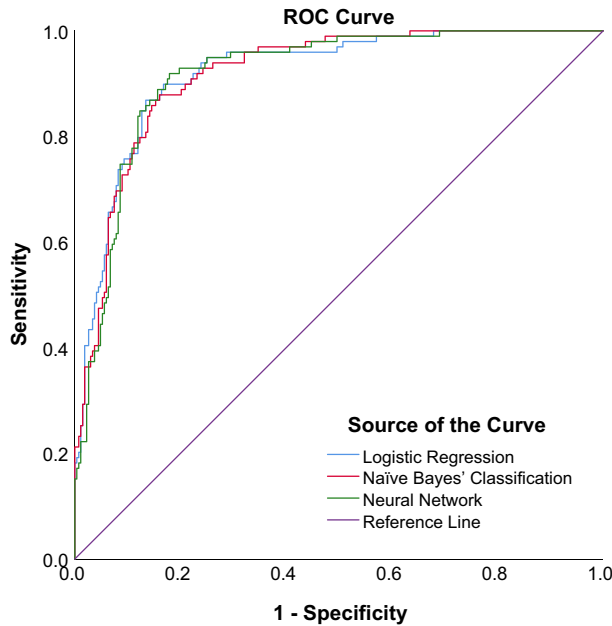
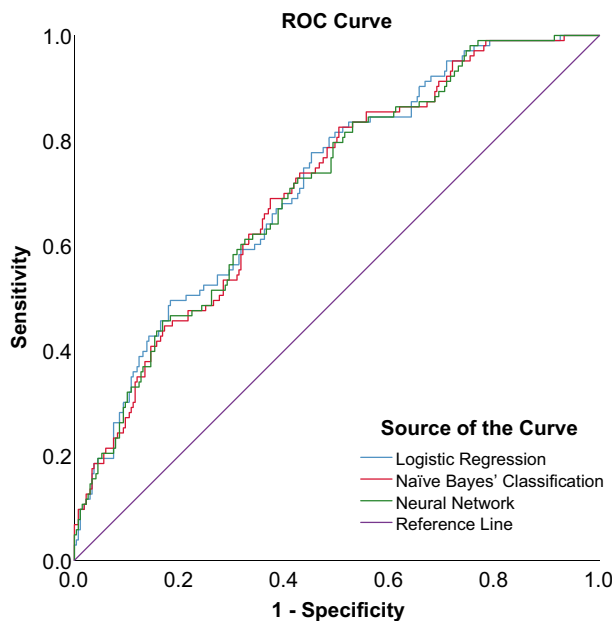**Fig. 5.** ROC curves of three prediction models in PACS eyes with pupillary block.

Fig. 6. ROC curves of three prediction models in PACS eyes with plateau iris configuration.

determined as AOD500 in light (p = 0.026), ARA750 in light (p < 0.001) and IA change/PD change (p = 0.029). In the TPIR group, the following three variables were selected: ARA750 in dark (p < 0.001), IT750 in dark (p < 0.001) and ACA in dark (p = 0.030). No significant collinearity among the input variables of each group was detected.

Figures 5, 6 and 7 show the ROC curves of the 3 algorithms in PB, PIC and TPIR groups, respectively. Table 6

shows the AUCs and 95% CIs of BLR, NBC and NN: in the PB group, these were 0.920, (95% CI, 0.890–0.950), 0.918 (95% CI, 0.889–0.947) and 0.917 (95% CI, 0.887–0.946), with no significant statistical differences (p = 0.990). The AUCs and 95% CIs of BLR, NBC and NN in PIC group were 0.715, (95% CI, 0.659–0.771), 0.708 (95% CI, 0.651–0.764) and 0.707 (95% CI, 0.650–0.764), with no significant statistical differences (p = 0.977). The AUCs and 95% CI

of BLR, NBC and NN in TPIR group were 0.867, (95% CI, 0.823–0.912), 0.833 (95% CI, 0.784–0.882) and 0.886 (95% CI, 0.849–0.922), respectively, with no significant statistical differences (p = 0.240). The sensitivity, specificity and the validation results (overall accuracy) of the three algorithms of each group with different AC mechanisms are also shown in Table 6.

Discussion

In a previous study, we had investigated algorithms for detection of PACS by combining static and dynamic ASOCT parameters and found that the three algorithms including BLR, NBC and NN failed to meet the requirements for population-based screening of PACS; NN had the largest AUC of 0.844 (Zhang et al. 2020). The current investigation shows potential for the development of an image-based non-contact method to screen for PACS, which is the ASOCT examinations under both light and dark conditions.

There are different AC mechanisms for PACD (Wang et al. 2000; Li et al. 2009). Pure pupillary block, pure non-pupillary block and combination of multiple mechanisms have been reported to underlie AC in Chinese eyes with PACD (Wang et al. 2000). In our previous study, we found that there were significant differences in ASOCT parameters between PACD eyes with different dominant AC mechanisms (Zhang et al. 2015). In another study, we also showed that the contribution of dynamic iris behaviour to the pathogenesis of PACD varies among those with different AC mechanisms (Zhang et al. 2015). Accordingly, we felt that using a single algorithm in detection of all PACS eyes might not be the best way to screen.

In this study, we categorized enrolled PACS eyes into three groups including PB, PIC and TPIR according to their dominant AC mechanisms as determined by ASOCT images. Among the three groups, PB group had the smallest IA change and IA change/PD change, suggesting that dynamic iris change has a more important role in angle closure where PB is the dominant AC mechanism; this is what we had found in our earlier study (Zhang et al. 2015). The reason for that may be the pressure gradient between the anterior
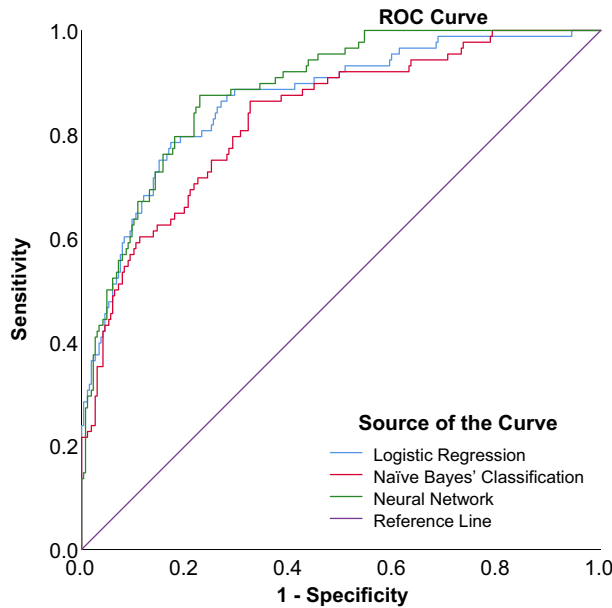
Fig. 7. ROC curves of three prediction models in PACS eyes with thick peripheral iris roll.

and posterior chambers in the PB group created by three forces including sphincter and dilator muscles as well as iris elasticity which affect the iris structure and change the capacity for free fluid movement (Nongpiur et al., 2011b; Zhang et al. 2015).

The three algorithms demonstrated good AUCs in the PB group, moderate AUCs in TPIR group and relatively poor AUCs in PIC group. In our previous study, the largest AUC (0.844) was for NN for detection of all PACS eyes; this is less than that for the PB and TPIR groups and better than that for the PIC group. We evaluated the performance of three prediction models in detection of PACS as a new method of screening for PACD based on different AC mechanisms. This method performed best in detection of PACS with PB as the dominant AC mechanism.

Early diagnosis of PACD can be achieved by population-based screening or case detection (opportunistic screening) (Thomas et al. 2002). Our findings suggest that this new method (prediction models using variables obtained through ASOCT measurements in both dark and light conditions) was suitable for population-based screening as well as in case detection of PACS eyes with PB as the dominant AC mechanism. And this method (prediction models using variables obtained through ASOCT measurements in dark conditions) may have potential use in case detection of PACS eyes with TPIR as the dominant AC mechanism. The algorithm was not suitable for population-based screening or case detection in PACS eyes with PIC as the dominant AC mechanism.

The Zhongshan Angle-Closure Prevention (ZAP) trial reported a low

incidence of development of PAC or PACG in PACS subjects over 6 years and also suggested that performing LPI on a population basis may not be the best strategy for preventing visual impairment in PACS (He et al. 2019). Hence, population-based screening of PACS may seem insignificant based on those findings. However, the ZAP trial fails to provide sufficient information referring to the risk which is especially important in determining whether an individual PACS is with higher possibility of a sight-threatening acute attack and should undergo a prophylactic LPI (He et al. 2019).

We believe that early screening for PACS is not useless; identifying and targeting which PACS are at higher risk of developing angle closure or vision-impairing acute attack are essential and also the most powerful tool for preventing blindness and low vision caused by PACD.

The ultimate goal of our study is looking for an ideal screening method for all stages of PACD, not only for PACS. However, as our study was based on a population-based research (follow-up of the Handan Eye Study), the number of PAC or PACG was very limited. We intended to establish and evaluate this new method first in PACS cases; in a future study, we will further evaluate the performance of this method in PAC/PACG cases.

Previous studies have reported that the AC mechanism involved in most AAC eyes and fellow eyes of AAC is predominantly PB, while non-pupillary block or multiple mechanisms have a greater role in non-acute presentations (Barkan 1954; Zhou et al. 1993; Moghimi et al. 2018). Acute angle-closure (AAC) is a subtype of PACD and an ocular emergency which in the

Table 6. AUC, sensitivity and specificity of algorithms.

Angle-closure mechanisms	Prediction algorithm	Overall accuracy (%)	AUC	95% CI of AUC	sensitivity	95% CI of sensitivity	specificity	95% CI of specificity
Pupillary Block	LR	80.9	0.920	0.890, 0.950	86.87%	84.81%, 88.93%	86.57%	83.14%, 89.99%
	NBC	77.7	0.918	0.889, 0.947	87.88%	85.89%, 89.87%	83.96%	80.27%, 87.64%
	NN	82.1	0.917	0.887, 0.946	88.89%	86.97%, 90.81%	84.33%	80.67%, 87.98%
Plateau Iris Configuration	LR	66.0	0.715	0.659, 0.771	77.67%	75.13%, 80.21%	54.85%	49.95%, 59.75%
	NBC	68.6	0.708	0.651, 0.764	68.93%	66.11%, 71.76%	62.69%	57.92%, 67.45%
	NN	74.7	0.707	0.650, 0.764	68.93%	66.11%, 71.76%	60.45%	55.63%, 65.27%
Thick Peripheral Iris Roll	LR	79.6	0.867	0.823, 0.912	78.41%	75.90%, 80.92%	82.84%	78.82%, 86.86%
	NBC	73.7	0.833	0.784, 0.882	86.36%	84.27%, 88.46%	67.54%	62.55%, 72.53%
	NN	86.8	0.886	0.849, 0.922	87.50%	85.48%, 89.52%	77.24%	72.77%, 81.71%

AUC = area under the receiver operator characteristic curve, CI = confidence interval, LR = logistic regression, NBC = Naïve Bayes' classification, NN = neural network.

absence of timely treatment causes permanent visual loss (Ha et al. 2019).

Early screening for AAC would be beneficial. We found that the new method which was based on algorithms and combination of anatomical and dynamic ASOCT parameters performed well in detection of PACS with PB as the dominant AC mechanism and may be helpful in screening eyes which are at risk of AAC. This would require confirmation by a prospective study.

Gonioscopy certainly remains the primary method for angle assessment and the gold standard for the diagnosis of PACD and is essential when the decision of how to manage an individual with PACD is made. However, even in the clinics, gonioscopy is not performed half of the time probably due to lack of experience, potential discomfort and lack of time (Chansangpetch et al. 2018). And its fair inter- and intra-observer reproducibility, situations such as corneal pathologies or uncooperative patients prevents it from being an ideal screening, detecting and monitoring method for angle closure (Chansangpetch et al. 2018).

The anterior segment imaging machines such as ASOCT are now already commonly available in more developed areas. In developing areas and countries such as China, ASOCT will become more and more common with the development of economics and medical resources, which makes it a preferable option for early screening of PACD. For underdeveloped countries and areas where ASOCT is not practical for screening for its high costs, gonioscopy is still more suitable for its characteristics of being cost-effective and portable (Chansangpetch et al. 2018).

Our study has several strengths. To the best of our knowledge, it is the first study to establish and evaluate a novel method for detection of PACS with different AC mechanisms by combining multiple static and dynamic anterior segment parameters on the basis of three prediction algorithms. Our analysis used the ISGEO classification system for PACD. Anterior segment optical coherence tomography (ASOCT), which is non-contact, eliminates patient discomfort and inadvertent compression of the globe and has the advantages of ease of operation, rapidity of image acquisition, less inter-

operator variability and angle viewing in its natural state because of the use of infrared light (Angmo et al. 2016).

The study has several limitations. Firstly, we included only PACS eyes but not those with established primary angle closure because the decision to treat is evident in the latter. This makes it difficult to estimate how eyes with confirmed angle closure would respond. Secondly, our subjects were Chinese and caution is warranted in extrapolating the findings to other ethnic groups. Thirdly, subjects with limbal anterior chamber depth ≤40% and had undergone gonioscopic examination and ASOCT imaging under light and dark conditions were enrolled in our study, which may cause some bias when drawing a conclusion. In the future, we would further assess this screening method in general population. Fourthly, the main disadvantage of ASOCT is the inability to image structures posterior to the iris such as the posterior chamber of the eye, zonules and the ciliary body (Nongpiur et al. 2020). Therefore, mechanisms of angle closure effected by ciliary body components such as plateau iris may not be wholly elucidated with ASOCT (Nongpiur et al. 2020). Our earlier study did find a good kappa (0.870) with the UBM for the same observer in determination of the AC mechanism (Zhang et al. 2016). Also, the Visante ASOCT could not perform the 360-degree imaging of the entire anterior chamber, which may miss some information. Also, currently available software analysis programmes are semiautomated and require manual localization of the scleral spur (Quek et al. 2011). This can be difficult especially in closed angles or where there is a smooth transition from cornea to sclera (Quek et al. 2011). We are planning a study to investigate fully automated image analysis software for angle-closure detection. Finally, external validation which requires evaluation of the performance of these models in other participant data is needed.

Conclusions

In summary, we compared three prediction models derived from static and dynamic ASOCT-based parameters obtained under both light and dark conditions for the detection of PACS

with different dominant AC mechanisms. This new method showed the best performance for detection of PACS with pupillary block mechanism with potential for use in population-based screening as well as in case detection. In a future study, we plan to enrol PACD patients from clinics at our hospital and further evaluate the performance of these models in screening of PACD in the real world.

References

Angmo D, Nongpiur ME, Sharma R, Sidhu T, Sihota R & Dada T (2016): Clinical utility of anterior segment swept-source optical coherence tomography in glaucoma. Oman J Ophthalmol 9: 3–10.

Barkan O (1954): Narrow-angle glaucoma; pupillary block and the narrow-angle mechanism. Am J Ophthalmol 37: 332–350.

Chansangpetch S, Rojanapongpun P & Lin SC (2018): Anterior segment imaging for angle closure. Am J Ophthalmol 188: xvi–xxix.

Console JW, Sakata LM, Aung T, Friedman DS & He M (2008): Quantitative analysis of anterior segment optical coherence tomography images: the Zhongshan Angle Assessment Program. Br J Ophthalmol 92: 1612–1616.

Cox DR (1958): The regression analysis of binary sequences (with discussion). J Roy Stat Soc B 20: 215–242.

Dorairaj S, Tsai JC & Grippo TM (2012): Changing trends of imaging in angle closure evaluation. ISRN Ophthalmol 2012: 597124.

Dreiseitl S & Ohno-Machado L (2002): Logistic regression and artificial neural network classification models: a methodology review. J Biomed Inform 35: 352–359.

Fluss R, Faraggi D & Reiser B (2005): Estimation of the Youden Index and its associated cutoff point. Biom J 47: 458–472.

Ford E, Rooney P, Oliver S, Hoile R, Hurley P, Banerjee S, van Marwijk H & Cassell J (2019): Identifying undetected dementia in UK primary care patients: a retrospective case control study comparing machine-learning and standard epidemiological approaches. BMC Med Inform Decis Mak 19: 248.

Foster PJ, Buhrmann R, Quigley HA & Johnson GJ (2002): The definition and classification of glaucoma in prevalence surveys. Br J Ophthalmol 86: 238–242.

Friedman DS & He M (2008): Anterior chamber angle assessment techniques. Surv Ophthalmol 53: 250–273.

Fu H, Xu Y, Lin S, Wong DWK, Baskaran M, Mahesh M, Aung T & Liu J (2019): Angle-closure detection in anterior segment OCT based on multilevel deep network. IEEE Trans Cybern 50: 3358–3366. https://doi.org/10.1109/TCYB.2019.2897162.

Ha JY, Sung MS, Heo H & Park SW (2019): Trends in the characteristics of acute

primary angle closure in Korea over the past 10-years. PLoS One 14: e0223527.

Hassoun MH (1995): Fundamentals of artificial neural networks. Cambridge, MA: The MIT Press.

Hastie T, Tibshirani R & Friedman J (2009): The Elements of Statistical Learning: Data Mining, Inference, and Prediction, 2nd edn. New York: Springer.

He M, Jiang Y, Huang S, Chang DS, Munoz B, Aung T, Foster PJ & Friedman DS (2019): Laser peripheral iridotomy for the prevention of angle closure: a single-centre, randomised controlled trial. Lancet 393: 1609–1618.

Jamal S, Khubaib M, Gangwar R, Grover S, Grover A & Hasnain SE (2020): Artificial Intelligence and Machine learning based prediction of resistant and susceptible mutations in Mycobacterium tuberculosis. Sci Rep 10: 5487.

Lavanya R, Foster PJ, Sakata LM et al. (2008): Screening for narrow angles in the Singapore population: evaluation of new noncontact screening methods. Ophthalmology 115: 1720–1727.

Li SZ, Liang YB, Fan SJ et al. (2009): Mechanism of angle-closure in patients with narrow angle in Handan Area with ultrasound biomicroscopy. Chinese J Pract Ophthalmol 27: 445–447.

McCallum A & Nigam K. (1998): A comparison of event models for Naive Bayes text classification. In Proc. of the AAAI-98 Workshop on Learning for Text Categorization 41–48.

Moghimi S, Torkashvand A, Mohammadi M, Yaseri M, Saunders LJ, Lin SC & Weinreb RN (2018): Classification of primary angle closure spectrum with hierarchical cluster analysis. PLoS One 13: e0199157.

Moghimi S, Vahedian Z, Fakhraie G et al. (2013): Ocular biometry in the subtypes of angle closure: an anterior segment optical coherence tomography study. Am J Ophthalmol 155: 664–673.

Nongpiur ME, He MG, Amerasinghe N et al. (2011): Lens vault, thickness and position in Chinese subjects with angle closure. Ophthalmology 118: 474–479.

Nongpiur ME, Ku JY & Aung T (2011): Angle closure glaucoma: a mechanistic review. Curr Opin Ophthalmol 22: 96–101.

Nongpiur ME, Sakata LM, Friedman DS, He M, Chan YH, Lavanya R, Wong TY & Aung T (2010): Novel association of smaller anterior chamber width with angle closure in Singaporeans. Ophthalmology 117: 1967–1973.

Nongpiur M, Tun TA & Aung T (2020): Anterior segment optical coherence tomography: is there a clinical role in management of primary angle closure disease? J Glaucoma 29: 60–66.

Qiao Y, Tan C, Zhang M, Sun X & Chen J (2019): Comparison of spectral domain and swept source optical coherence tomography for angle assessment of Chinese elderly subjects. BMC Ophthalmol 19: 142.

Quek DT, Nongpiur ME, Perera SA & Aung T (2011): Angle imaging: Advances and challenges. Indian J Ophthalmol 59(Suppl): S69–75.

Quigley HA & Broman AT (2006): The number of people with glaucoma worldwide in 2010 and 2020. Br J Ophthalmol 90: 262–267.

Radhakrishnan S, Rollins AM, Roth JE, Yazdanfar S, Westphal V, Bardenstein DS & Izatt JA (2001): Real time optical coherence tomography of the anterior segment at 1310 nm. Arch Ophthalmol 119: 1179–1185.

Sakata LM, Lavanya R, Friedman DS, Aung HT, Seah SK, Foster PJ & Aung T (2008): Assessment of the scleral spur in anterior segment optical coherence tomography images. Arch Ophthalmol 126: 181–185.

Salim S (2012): The role of anterior segment optical coherence tomography in glaucoma. J Ophthalmol 2012: 476801.

Sun JH, Sung KR, Yun SC, Cheon MH, Tchah HW, Kim MJ & Kim JY (2012): Factors associated with anterior chamber narrowing with age: an optical coherence tomography study. Invest Ophthalmol Vis Sci 53: 2607–2610.

Tham YC, Li X, Wong TY, Quigley HA, Aung T & Cheng CY (2014): Global prevalence of glaucoma and projections of glaucoma burden through 2040: a systematic review and meta-analysis. Ophthalmology 121: 2081–2090.

Thomas R, Parikh R, Paul P & Muliyil J (2002): Population-based screening versus case detection. Indian J Ophthalmol 50: 233–237.

Wang YE, Li Y, Wang D, He M & Lin S (2013): Comparison of factors associated with occludable angle between American Caucasians and ethnic Chinese. Invest Ophthalmol Vis Sci 54: 7717–7723.

Wang N, Ouyang J, Zhou W, Lai M, Ye T, Zeng M & Chen J. (2000): Multiple patterns of angle closure mechanisms in primary angle closure glaucoma in Chinese. Zhonghua Yan Ke Za Zhi 36: 46–51, 5, 6.

Wang D, Qi M, He M, Wu L & Lin S (2012): Ethnic difference of the anterior chamber area and volume and its association with angle width. Invest Ophthalmol Vis Sci 53: 3139–3144.

Weinreb N, Friedman D & authors, (2006): Angle closure and angle closure glaucoma. The Hauge, The Netherlands: Kugler Publications.

Zhang Y, Li SZ, Li L, He MG, Thomas R & Wang NL (2015): Quantitative analysis of iris changes following mydriasis in subjects with different mechanisms of angle closure. Invest Ophthalmol Vis Sci 56: 563–570.

Zhang Y, Li SZ, Li L, Thomas R & Wang NL (2014): The handan eye study: comparison of screening methods for primary angle closure suspects in a rural Chinese population. Ophthalmic Epidemiol 21: 268–275.

Zhang Y, Tang X & Wang NL (2016): The reproducibility of mechanism categories of angle closure using ultrasound biomicroscopy and anterior segment optical coherence tomography. Chin J Exp Ophthalmol 34: 936–940.

Zhang Y, Zhang Q, Li L, Thomas R, Li SZ, He MG & Wang NL (2020): Establishment and comparison of algorithms for detection of primary angle closure suspect based on static and dynamic anterior segment parameters. Trans Vis Sci Tech 9: 16. (Accepted).

Zhou WB, Li MY & Wang ZH (1993): Advances in the Glaucoma Research. Shandong: Qingdao Ocean Press, pp. 43–45.

Correspondence:
Ningli Wang, MD, PhD
Beijing Institute of Ophthalmology
Beijing Tongren Eye Center
Beijing Tongren Hospital
Capital Medical University
Beijing
China
Tel: +86-1058269920
Fax: +86-1058269920
Email: wningli@vip.163.com

†These two authors contribute equally to this work.